American Mineralogist, Volume 76, pages 733–742, 1991

Bonding and elasticity of stishovite SiO_2 at high pressure: Linearized augmented plane wave calculations

Ronald E. Cohen
Geophysical Laboratory, Carnegie Institution of Washington, 5251 Broad Branch Road, NW, Washington, DC 20015, U.S.A.

Abstract

The crystal structure, equation-of-state, elasticity, A_{1g} Raman mode, and electronic structure of stishovite (rutile-structured SiO_2) are studied at high pressure from first principles using the linearized augmented plane wave (LAPW) method. Excellent agreement is found with the experimentally known properties. The pressure dependence of three elastic constants is predicted. The charge density and band structure indicate a mixture of ionic and covalent bonding in stishovite, and the ionicity is quantitatively estimated. No major changes in bonding are found between zero pressure and 150 GPa.

Introduction

Stishovite is the simplest silicate with octahedrally coordinated Si and thus is of great interest, both theoretically and experimentally, as a prototype for high-pressure silicate phases that are important in Earth's lower mantle. Furthermore, it is of crystal chemical interest to understand the bonding and electronic structure and, in particular, the ionicity and covalency of the Si-O bond, in a dense octahedrally coordinated phase. A theoretical study of stishovite is particularly suited for this honorary volume, because the existence of a rutile-structured form of SiO_2 was predicted by James B. Thompson, Jr. in the early 1950s (Birch, p. 234 and 274, 1952). Such a phase was not synthesized until 1961 (Stishov and Popova, 1961), shortly after which the mineral was discovered at Meteor Crater, Arizona (Chao et al., 1962).

Numerous experimental data are available for stishovite at various pressures, including Raman frequencies (Hemley et al., 1986; Hemley, 1987), X-ray diffraction data (Liu et al., 1974; Sato, 1977; Endo et al., 1986), precise electron density maps derived from X-ray diffraction (Spackman et al., 1987), and single-crystal elastic constants determined from Brillouin scattering (Weidner et al., 1982); all of these can be compared with results of first-principle calculations. Theoretical studies of stishovite include empirical models (Erikson and Hostetler, 1987), ab initio models such as the potential induced breathing (PIB) model (Cohen 1987a), models based on molecular orbital theory (Burdett, 1985; Lasaga and Gibbs, 1987; Tsuneyuki et al., 1988, 1989), linearized augmented plane wave (LAPW) calculations investigating possible high-pressure phase transitions (Park et al., 1988), and Hartree-Fock crystal calculations at zero pressure (Nada et al., 1990). Recently a reversible high-pressure phase transition from stishovite to a $CaCl_2$ structure was claimed by Tsuchida and Yagi (1989) at pressures of 80–100 GPa in a laser-heated diamond anvil cell.

First-principle calculations of the properties of crystals are complementary to experimental studies. The purpose of these calculations is not merely to compare results with experimental data but to make predictions and to increase understanding of the origin of the behavior of solids. Only recently has it become possible to study the elastic, optical, and electronic properties of complex crystals such as stishovite, making no approximations except for a local approximation for the exchange and correlation interactions between electrons. Although this local density approximation (LDA) is a rather severe approximation, in general it gives excellent results for ground state properties, with errors of up to a few percent in lattice parameters and usually better than 15% in the bulk modulus. The occupied electronic bands are usually in very good agreement with experiment. The main problems with the LDA occur in systems such as FeO and La_2CuO_4, where the LDA incorrectly predicts metallic rather than insulating behavior because antiferromagnetic susceptibility is underestimated.

In contrast to model calculations, no assumptions about such characteristics as ionicity and covalency are made, and the only inputs are the nuclear charges and masses. With only these inputs, the total static crystal energy can be calculated as a function of the nuclear positions. If one is interested in the properties of a given (either experimentally known or hypothetical) crystal, one uses the symmetry constraints for the given space group to simplify the calculation. The choice of symmetry, however, is not an essential feature, and symmetry constraints can be relaxed completely, except for translation symmetry, when studying a bulk crystalline solid. Vibrational and elastic properties can be studied by calculating the energy as a function of strain or internal structural parameters.

Here the elastic and vibrational properties that can be obtained by distortions of stishovite without lowering the space group symmetry, *Pnnm*, are considered. By inducing such strains and distortions, the fully symmetric, A_{1g}, Raman frequency and its Gruneisen parameter, γ, the elastic constants $C_{11} + C_{12}$, C_{33}, C_{13} (which also deter-

0003–004X/91/0506–0733$02.00

mine the bulk modulus K and the linear compressabilities k_a and k_c), the structural parameter c/a, the O positional parameter x(O) [the O equipoint is at (xx0)], and the volume can be determined as functions of pressure. These quantities can be compared with experimental data where such data are available, and they form first-principle predictions in the absence of data. For example, the high-pressure elastic properties of stishovite are unknown. In addition to the elastic, vibrational, and structural quantities that can be calculated, both the charge density and the band structure can be investigated as functions of pressure. Both the total energy and the charge density results can be used as benchmarks for the formulation of better models that could then be used to calculate thermoelastic properties of stishovite.

LDA AND THE LAPW METHOD

The calculations discussed here are based on the density functional theory of Hohenberg and Kohn (1964) and Kohn and Sham (1965). The basic idea is that the exact ground state properties of a substance, including the ground state energy, are functionals of the charge density alone. Kohn and Sham showed how to calculate the ground-state charge density and total energy by solving a set of single-particle Schrödinger-like equations, $H\psi_i(k) = \epsilon_i(k)\psi_i(k)$ self-consistently, with a Hamiltonian given by

$$H = -\frac{\hbar^2}{2m}\nabla^2 + V_{ext} + V_{xc} \quad (1)$$

where V_{ext} is the nuclear electrostatic potential and V_{xc} is the exchange-correlation potential. The total energy is given by

$$E = T + U + E_{xc} \quad (2)$$

where T is the kinetic energy of a system of noninteracting electrons with the same density as the interacting system, U is the electrostatic (Hartree) energy including the electrostatic energy between the nuclei, and E_{xc} is the exchange-correlation energy. The beauty of the method is that the exact, many-body ground state energy can be found by solving a set of single-particle equations. Unfortunately, the exact solution requires the exact exchange-correlation functional, which is unknown and undoubtedly extremely complicated and nonlocal. Fortunately, a simple functional based on the homogeneous electron gas works very well, at least for nonmagnetic systems. In this approximation, one simply uses a local exchange-correlation potential that corresponds at each point in space to the exchange-correlation functional appropriate to a homogeneous electron gas with a density corresponding to the charge density at that point in space. This is known as the local density approximation (LDA). The Hedin-Lundqvist (1971) parameterization of the exchange-correlation functional is used here. Reviews of the LDA are given by Pickett (1985) and Schluter and Sham (1982).

The LAPW method (Wei and Krakauer, 1985) is one of the most accurate for solution of the Kohn-Sham equations within the local density approximation. All types of crystals, whether bonding is ionic, metallic, or covalent and no matter which elements in the periodic table they contain, can be treated on the same footing. This is an all-electron method that makes no shape approximations for the charge density or the potential and that can be essentially fully converged. Space is divided into two types of regions: the volumes inside spherical "muffin tins" surrounding each nucleus and the interstitial volume between the muffin tins. Within the muffin tins, the radial functions are represented as linear combinations of solutions of the radial Schrödinger's equation for an energy E_i for each orbital and its energy derivative in a spherical potential. Different energy parameters E_i can be used in separate energy windows. Nonspherical terms are represented in terms of sums of spherical harmonics. In the interstitial region, a plane wave expansion is used. The plane waves are joined smoothly onto the expansion inside the muffin tins. The one approximation inherent in the method is that the basis functions inside the sphere are not a complete set. The basis functions in each sphere are the eigensolutions of the sphericalized potential, rather than the actual nonspherical crystal potential inside the spheres. (Note that this is only to form the basis functions; the full nonspherical potential is used to diagonalize the problem within the LAPW basis set.) Also, only a single set of orbitals with a given angular momentum is used inside a given energy window. This can cause problems when high-lying semi-core states with a given angular momentum are present below the valence band where the same angular momenta are important; the lower states can be picked up below the energy window, effectively reducing the variational freedom to describe the valence states. This is a technical issue that leads to greater complexity in the calculations but fortunately does not arise at all in SiO_2. The former approximation is not known to cause problems even in the most nonspherical systems.

The time-consuming steps are the setup of the Hamiltonian ($H_{ij} = \langle i|H|j\rangle$) and overlap ($O_{ij} = \langle i|j\rangle$) matrices and the diagonalization of the secular equation

$$\sum_j H_{ij}\psi_j(\mathbf{k}) = \sum_j e_i(\mathbf{k})\, O_{ij}\psi_j(\mathbf{k}).$$

The charge density is given by

$$\rho = \int d\mathbf{k} \sum_{occ} \psi_i^*(\mathbf{k})\psi_i(\mathbf{k}) \quad (3)$$

where the integral is over the Brillouin zone and is replaced by a discrete sum over a set of special k-points in the irreducible wedge of the Brillouin zone, i is the band index, and the sum is for occupied states. Typically there are 70–150 basis functions per atom in the unit cell. A

Table 1. Equation-of-state, structural parameters, and A_{1g} Raman frequency for stishovite

V (Bohr^3)	V (Å^3)	$E + 1755$ (Ryd)	P (GPa)	c/a	x	ν (cm^{-1})
240	35.56	−0.0915	143	0.6548	0.3002	1102
260	38.53	−0.2440	84	0.6535	0.3013	983
280	41.49	−0.3290	43	0.6516	0.3025	873
300	44.45	−0.3660	13	0.6460	0.3042	808
314	46.53	−0.3708	−2.5	0.6404	0.3057	751
320	47.42	−0.3686	−8.2	0.6361	0.3066	727

setup and diagonalization has to be performed for each k-point in the sum over the Brillouin zone. For maximum accuracy, at least two windows are used, with a separate basis set for each window. The valence states are treated in one window and the semicore states are treated in another window. (This still allows the states to hybridize but in general increases the accuracy by linearizing the basis functions around energy parameters in each window.) The deep core states are treated by solution of the Dirac equation in the potential of all of the electrons. The core states are thus treated fully relativistically, and the semicore and valence states are treated semi-(scalar) relativistically. Approximately ten iterations are required to reach self-consistency.

The LAPW method has been used to study the energetics of several oxides. Mehl et al. (1988) studied the equations-of-state of MgO and CaO and predicted a phase transition from the NaCl structure (B1) to the CsCl structure (B2) in MgO at 510 GPa. Cohen et al. (1989a, 1990a) calculated vibrational frequencies in La_2CuO_4, Cohen et al. (1990b) calculated all 15 Raman frequencies and eigenvectors in $YBa_2Cu_3O_7$, and Cohen et al. (1989b) calculated the equation of state of $MgSiO_3$ perovskite using the LAPW method. Park et al. (1988) studied possible phase transitions in stishovite using the LAPW. Mehl et al. (1990) demonstrated that elastic constants can be reliably calculated in intermetallic alloys using the LAPW method.

Total energy calculations and results

For stishovite, the O 2s states were treated in a separate semicore energy window and the hybrid O 2p–Si valence states in a valence window. (The use of two windows is only to decrease any errors caused by the linearization of the basis functions with respect to energy. It does not assume that the semicore and valence states do not interact. Also, the presence of O 2s and hybrid O 2p and Si band states is never assumed. That is a product of the computations and agrees with chemical intuition.) The deeper states were treated as core states. A convergence parameter $RK_{max} = 7$ was found to be sufficient, which gives about 540 (90/atom) LAPW basis functions at zero pressure. The nonspherical potential and charge density were expanded to an angular momentum $l = 8$. To perform the Brillouin zone sums such as Equation 3, a (444) special k-point mesh was used which gives six special k-points for each energy window. The total energy was

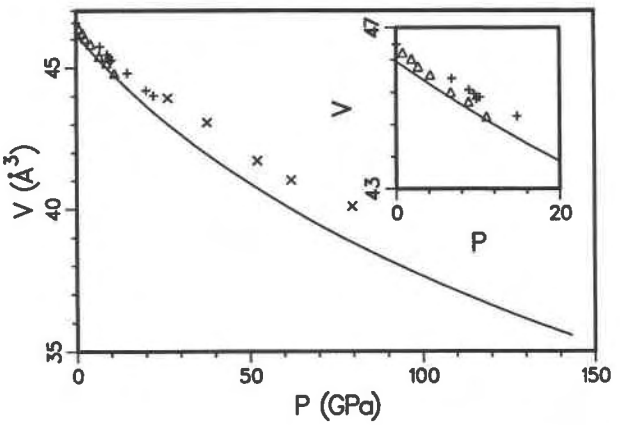

Fig. 1. Equation-of-state of stishovite. The solid curve is the LAPW equation-of-state, and the symbols represent the following experimental data: +, Liu et al. (1974); △, Sato (1977); ×, Tsuchida and Yagi (1989).

calculated as a function of c/a and x(O) for six volumes from 35.56 to 47.42 Å^3. Calculations for at least three values of x were performed at each value of c/a and for at least three values of c/a at each volume.

Structure and equation-of-state

The calculated energies at each volume and c/a were fitted to a polynomial as a function of the parameter x, and then the minimum energies with respect to x were fitted as functions of c/a at each volume. In this way, the minimum energy as a function of volume as well as the structural parameters c/a and x were determined (Table 1). The total energies as a function of volume were then fitted to a third-order Birch equation (Birch, 1978) to obtain the equation-of-state and the parameters V_o, K_o, and K_o'. The resulting equation-of-state gives a zero pressure volume V_o of 46.16 Å^3, bulk modulus K_o of 324 GPa, and bulk modulus pressure derivative K_o' of 4.04. A fit to the Murnaghan equation-of-state gives $V_o = 46.16$ Å^3, $K_o = 329$ GPa, and $K_o' = 3.66$. Figure 1 shows the calculated equation-of-state compared with experimental data. The higher pressure data of Tsuchida and Yagi (1989) are systematically displaced from both the predicted equation-of-state and extrapolated equations-of-state of the lower pressure studies. This may reflect significant nonhydrostaticity, as suggested in their paper, or error in the lattice parameters derived from four to six diffraction lines, or both. A Murnaghan equation-of-state fit to their data gives $K_o = 407$ GPa and $K_o' = 3.2$ ($K_o = 376$ GPa if K' is fixed at 4). This bulk modulus is significantly higher than that obtained by other studies (Table 2).

The present LAPW results differ somewhat from the LAPW results of Park et al. (1988), who found $V_o = 47.51$ Å^3, $K_o = 288$ GPa, and $K_o' = 3.14$ using a Murnaghan equation-of-state. This difference may simply be because Park et al. (1988) fitted their results over a different range

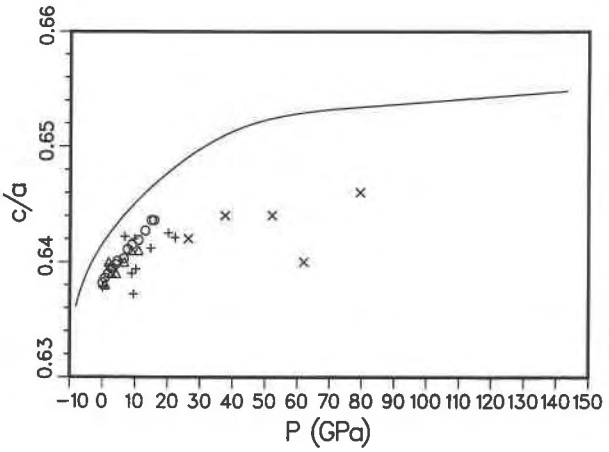

Fig. 2. The axial ratio c/a vs. pressure. Symbols are the same as for Figure 1, plus ○, which represents data from Ross et al. (1990).

of volume, used one energy window, or used a different exchange-correlation functional.

The present LAPW equation-of-state is in good agreement with experiment (Table 2). It is evident from the large error bars that there is essentially no information on the bulk modulus derivative K_o'. Even the very high pressure equation-of-state to 75 GPa determined in the diamond anvil cell by Tsuchida and Yagi (1989) cannot constrain K_o' well because of the nonhydrostatic conditions and the relatively large uncertainty in the volume and pressure at the highest pressures. The LAPW static zero-pressure bulk modulus, 324 GPa, is slightly higher than the experimental room temperature values, but at the experimental zero-pressure volume, the present LAPW value of 314 GPa is quite close to the experimental value derived from the single crystal elastic constants of 306 ± 4 (Weidner et al., 1982).

TABLE 2. Comparison of equation-of-state and zero-pressure structure parameters with experimental values

	LAPW Present study static	LAPW Park et al. (1988) static	Experiment (300 K)
V_o Å^3	46.16	47.51	46.60[A]
K_o GPa	324	288	344 ± 27[A]
			292 ± 9[B,C]
			294 ± 14[D,C]
			306 ± 4[E]
K_o'	4.04	3.14	3.1 ± 3.7[B,C]
			3.2 ± 3.3[D,C]
			2.8 ± 0.2[F]
c/a	0.640		0.638[G]
x(O)	0.306		0.306[G]

[A] Liu et al. (1974).
[B] Sato (1977).
[C] Reanalyzed by Bass et al. (1981).
[D] Olinger (1976).
[E] Weidner et al. (1982).
[F] Ross et al. (1990).
[G] Spackman et al. (1987).

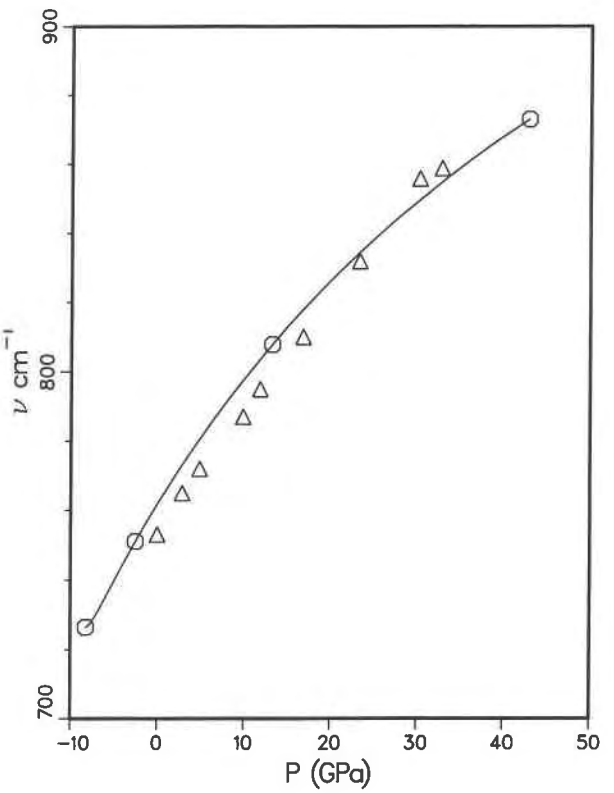

Fig. 3. Pressure dependence of the A_{1g} Raman frequency for stishovite. The experimental data (△) are from Hemley (1987).

The structural parameters c/a and x (O) agree well with experiment at zero pressure. Figure 2 compares the calculated with experimental c/a ratio as functions of pressure. The lattice parameters of Tsuchida and Yagi seem to be less reliable, perhaps because of large nonhydrostatic stresses compared with either the trends in lower pressure data or with the LAPW results. The observed and predicted c/a values could be combined with the elastic constants (derived below) to estimate the nonhydrostatic stresses. The calculated decrease in c/a with increasing volume is consistent with the high-temperature study of Ito et al. (1974), in which c/a decreased by 0.29% from 291 K to 873 K.

A_{1g} Raman frequency

Table 1 and Figure 3 show the calculated A_{1g} Raman frequency as a function of pressure. The zero-pressure A_{1g} frequency is calculated to be 751 cm^{-1}, in perfect agreement with the experimental value of 753 cm^{-1} (Hemley, 1987). (Here and below, when the LAPW results are compared with zero-pressure experimental quantities, the derived LAPW values are presented for the cell volume 46.53 Å^3, which corresponds to −2.5 GPa, to account for zero point and thermal pressure, which is probably roughly 2–3 GPa. This is a minor correction in any case.) The Gruneisen parameter $\gamma = -(\mathrm{d} \ln \nu / \mathrm{d} \ln V)$ was obtained by fitting $\ln \nu$ to a second order polynomial in $\ln V$ (with

TABLE 3. Derived values of elastic properties for stishovite

V (Bohr^3)	$k_a \times 10^4$	$k_c \times 10^4$	K	$1/(2k_a + k_c)$	C_s	C_{33}	C_{13}	$C_{11} + C_{12}$
240	5.15	3.08	840	747	246	1405	551	1612
260	4.95	5.22	638	661	188	1024	470	1524
280	7.47	5.76	489	483	173	889	327	1087
300	10.6	5.65	376	372	157	812	255	807
314	12.7	5.42	314	323	158	807	221	693
320	13.6	5.31	290	307	145	763	219	650

an rms error of 0.1%). The derived value $\gamma = 1.40$ is in excellent agreement with the experimental value 1.38 ± 0.04 obtained by Hemley (1987). The second derivative $(\mathrm{d}^2 \ln \nu/\mathrm{d} \ln V^2) = -(\mathrm{d} \ln \gamma/\mathrm{d} \ln V)$ is of interest since the thermodynamic Gruneisen parameter ν, which is important in the thermal equation of state, is related to the individual mode parameters, ν_i, and few or no experimental data are available to estimate its magnitude. The second derivative obtained is 0.14, which gives $\gamma = 1.47$ at 143 GPa.

Elasticity

In a crystal with Raman-active modes, the Raman modes couple with the elastic constants. Thus elastic constants cannot be obtained by simple homogeneous shears of the crystal lattice. It is necessary either to use the long-wavelength limit of lattice dynamics, as was done using the PIB model for stishovite by Cohen (1987a), or to minimize the energy as a function of internal atomic coordinates for each value of strain. Here the latter approach is used. The c/a strain at constant volume can be represented as the following strain tensor:

$$\epsilon = \begin{bmatrix} (\delta + 1)^{-1/3} - 1 & 0 & 0 \\ 0 & (\delta + 1)^{-1/3} - 1 & 0 \\ 0 & 0 & (\delta + 1)^{2/3} - 1 \end{bmatrix} \tag{4}$$

which is to linear order in δ:

$$\epsilon = \frac{1}{3}\begin{bmatrix} -\delta & 0 & 0 \\ 0 & -\delta & 0 \\ 0 & 0 & 2\delta \end{bmatrix}. \tag{5}$$

The new lattice parameters are given by $a' = (\epsilon + I)a$ where I is the identity matrix. The parameter δ is related to c/a by $(c/a) = (c/a)_o(1 + \delta)$ where $(c/a)_o$ is the equilibrium value of c/a at the given volume. Strains at constant volume (Eq. 4) were used here to find elastic constants, so no pressure terms arise in the analysis. Equation 5 was used to derive the values of the elastic constants, which is correct for the second-order elastic constants. The relationship between the second derivative of the energy with respect to strains is found from $\Delta E/V = \frac{1}{2} \Sigma\, C_{ij}\epsilon_i\epsilon_j$, using the Voigt notation (Nye, 1985). The result for a tetragonal crystal and the above strain is $\Delta E/V = (1/9)(C_{11} + 2C_{33} + C_{12} - 4C_{13})\delta^2 = C_s\delta^2$. The resulting values of C_s are given in Table 3 as functions of pressure. The elastic constants $C_{11} + C_{12}$, C_{33}, and C_{13} can be decoupled by using two of the following which have also been determined: the a and c linear compressibilities, k_a and k_c defined as for example $k_a = -\mathrm{d} \ln a/\mathrm{d}P$, and the bulk modulus K. These quantities are related by $K = 1/(2k_a + k_c)$. Here the linear compressibilities were obtained by fitting a third-order polynomial in the pressure to the natural logarithm of the lattice parameters, with the pressures obtained from the third-order Birch fit to the energies. This procedure is less reliable for the highest pressures because of the limited number of volumes studied. The bulk modulus K and $1/(2k_a + k_c)$ are compared in Table 3, and one finds reasonable correspondence between these two estimates. The linear compressibilities are related to the following elastic compliances (Nye, 1985):

$$\begin{aligned} k_a &= s_{11} + s_{12} + s_{13} \\ k_c &= 2s_{13} + s_{33}. \end{aligned} \tag{6}$$

The elastic compliances are related to the quantities C_s, k_a, and k_c by

$$\begin{aligned} s_{33} &= (4k_a + 2k_c + C_s k_c^2)/d \\ s_{13} &= (-2k_a - k_c + C_s k_a k_c)/d \\ s_{11} + s_{12} &= (2k_a + k_c + 2C_s k_a^2)/d \end{aligned} \tag{7}$$

where $d = 2C_s(k_a + k_c)$. The elastic constants can be found by inversion of the compliances. The results are shown in Table 3 and Figure 4.

The derived elastic constants can be compared with the single crystal Brillouin scattering results of Weidner et al. (1982) (Table 4). The elastic constants derived from the LAPW calculations are within a few percent of the experimental values, which is probably the limit of numerical accuracy of the calculations. Probably the LDA works so well for stishovite because it is rather stiff in terms of strains in volume and c/a, so that relatively large changes in energy are involved. There is no reason for the accuracy of LDA to decrease as pressure is increased, and in fact its accuracy may increase because the charge density becomes more uniform in the limit of very high pressures and energy differences become much larger.

The very small pressure derivative for C_s, which is approximately 0.2, is interesting because it may imply that the pressure dependence of the average shear modulus is

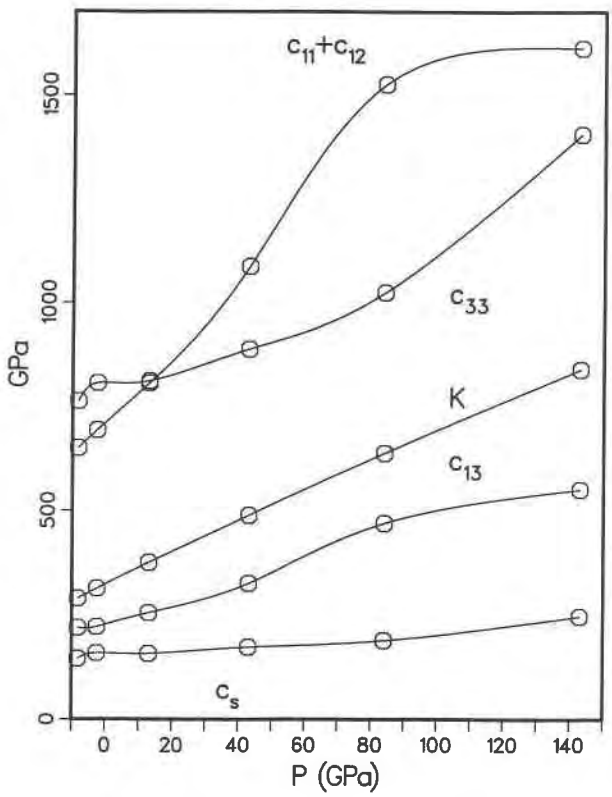

Fig. 4. Derived elastic constants for stishovite as functions of pressure.

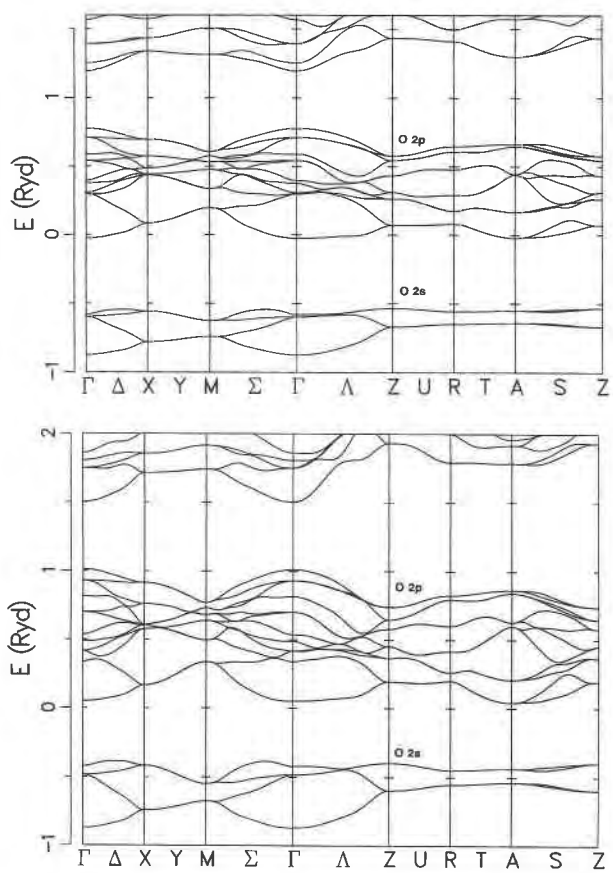

Fig. 5. Band structure for stishovite at **(top)** zero pressure and **(bottom)** 143 GPa. The labeled k-points are in units of (π/a,π/b,π/c), Γ (0,0,0), X (1,0,0), M (1,1,0), Z (0,0,1), R (1,0,1), and A (1,1,1).

small. The upper bound (Voigt approximation) for the average shear modulus for stishovite is $G_V = 0.3C_s + 0.1(C_{11} - C_{12}) + 0.4C_{44} + 0.2C_{66}$ (see Schreiber et al., 1973). The value of $C_s' = 0.2$ is smaller than the value of 1.3 predicted by the fully ionic PIB model calculations (Cohen, 1987a). The pressure derivative $(C_{11} - C_{12})'$ is calculated using the PIB model also to have a tiny pressure derivative (0.2), and $(C_{11} - C_{12})$ is actually expected to soften at high pressures because of the softening of the B_{1g} Raman mode (Hemley, 1987; Cohen, 1987a). Using the present value of C_s' and the PIB values of the other pressure derivatives gives $G_V' = 1.3$. The lower bound (Reuss bound) would be significantly less than 1 (the PIB lower bound for the shear modulus pressure derivative is 0.7), and the Reuss bound will go to zero as the B_{1g} mode softens before $C_{11} - C_{12}$ goes to zero. For comparison, the estimated G' is 1.7 for $MgSiO_3$ perovskite and 2.2 for MgO using the PIB model (Cohen 1987b). The small pressure derivatives of the shear modulus caution one not to rule out the possibility that stishovite exists in the lower mantle because of its relative stiffness at zero pressure; in other words, stishovite may stiffen more slowly with increasing pressure than other possible lower mantle phases.

TABLE 4. Comparison of calculated zero-pressure elastic properties with experimental values (GPa)

	LAPW	Weidner et al. (1982)	Ross et al. (1990)
C_s	158	156	
$C_{11} + C_{12}$	693	664	
C_{33}	807	776	
C_{13}	221	203	
$k_a \times 10^4$	12.7	13.2	11.9
$k_c \times 10^4$	5.42	6.0	6.8
K_0	314	308	313

Bonding and electron structure

Band structure and hybridization

Figure 5 shows the calculated band structure for stishovite at low and high pressures. The only qualitative changes in the band structure with pressure are general widening of the bands. The valence band consists primarily of O 2p states and is quite wide (11.2 eV at $P = 0$), but the dispersion of individual bands in the manifold is quite small. The small dispersion implies a localized ionic or atomic character, but the very large band width implies strong covalency, so that the mixed ionic-cova-

lent character of SiO_2 is evident in the stishovite band structure. The Si hybridization in the valence wavefunctions has s, p, and d character, and the decomposition of the resulting valence charge density at zero pressure consists of 0.19 s, 0.26 p, and 0.11 d electrons in each Si atomic sphere.

The O 2s band is also quite wide (4.4 eV), so one might be concerned about treating the O 2s states as core states in, for example, a pseudopotential calculation. The O 2s and valence states are well separated by a gap of 7.0 eV. The calculated band gap (which should be an underestimate with LDA (Pickett, 1985) is a direct gap at Γ of 5.7 eV. The band widths are in good agreement with the X-ray photoemission study of Wiech (1984) on stishovite; Wiech obtained an O 2s band width of 5.5 ± 0.6 eV and an O valence band width of 12 ± 0.6 eV, with a gap between of 5.5 ± 0.6 eV.

The valence band width increases from 11.2 at zero pressure to 13.1 eV at 143 GPa, the O 2s width increases from 4.4 to 6.8 eV, the gap between O 2s and O 2p decreases from 7.0 to 6.2 eV, and the band gap increases from 5.7 to 6.1 eV.

The latter observation is important because it indicates that the band gap of stishovite will not close at pressures existing in the earth. The band gap of MgO is also calculated to increase with pressure, but the gap of CaO decreases (Mehl et al., 1988). The band gap also increases with pressure in diamond (Fahey et al., 1987), but in most semiconductors the band gap shrinks with increasing pressure. Fahey et al. (1987) explained the positive pressure derivative of the diamond band gap by the absence of d-states with the same principal quantum number as the upper valence states. The same explanation might hold for SiO_2 and MgO. One cannot predict whether any silicates or oxides metallize in the earth at high pressures because of the presence of Ca and Fe, but metalization of magnesium silicates is unlikely.

The Hartree-Fock density of states (Nada et al., 1990) is qualitatively similar to the LDA and experiment but differs quantitatively, as expected. The Hartree-Fock valence band width is 14, compared with 11.2 eV, and the gap between the valence and O 2s bands is 10, rather than 7 eV. Nevertheless, the Hartree-Fock total energies give a good zero-pressure crystal structure for stishovite and give qualitatively similar charge density deformation maps.

Charge density

A more intuitive picture of bonding in stishovite can be obtained by examining the self-consistent charge density. It is difficult to obtain crystal charge densities experimentally because the interesting part of the charge density, that involved in the bonding, is superposed over spherical core densities that usually dominate the diffraction. Spackman et al. (1987) obtained a reliable experimental charge density for stishovite by using a combination of powder and single-crystal diffraction data and took great care to eliminate or correct for systematic errors. The atomic motions were removed from the experimental map by an anisotropic Debye-Waller treatment. They refined the nonspherical parts of the charge density alone, using standard sphericalized atomic densities for the spherical parts. Thus the experiment can contribute little regarding the relative ionicity of Si and O but can contribute much about the covalent bonding features. The experimental deformation densities are compared with the present calculations in Figure 6. Figures 6a and 6b show the axial and apical Si-O bonds, and Figures 6c and 6d show the O-O shared edge.

Very good qualitative agreement is found between the experimental deformation maps and the LAPW results. The main difference is that the calculation shows excess charge on the O and less on the Si than neutral atomic densities, as was assumed in the experimental study. Both the theoretical and experimental deformation densities show nonbonding O density perpendicular to the Si-O bond, and both give rise to about the same value of the peak bond charge density. It should be pointed out that the LAPW difference map was calculated using LDA spherical atoms as a reference density so that systematic differences in LDA and Hartree-Fock charge densities do not dominate the differences. Since the spherical part of the charge density was not determined in the experiment in any case, the choice of neutral spherical reference is somewhat arbitrary.

To explore the bonding in stishovite further, it is useful to have a reference density, unlike the reference neutral ions, that takes the ionicity into account. Furthermore, it is of interest to know what the effective ionicity is in stishovite in order to improve model calculations for high-pressure silicates. Cohen (1987a) used the nonempirical PIB model, with fully ionized Si^{4+} and O^{2-}, and obtained elastic constants significantly higher than experimental values. One possible source of the large discrepancies was the neglect of covalency and the use of fully ionized species. Therefore, the self-consistent charge density is compared with PIB charge densities generated using O charges from −2 to −1.2 and Si charges to compensate. The Si ion charge densities were calculated with partial occupancy of the Si 3s states and calculating a spherically averaged charge density self-consistently. Each O ion charge density was calculated self-consistently as in the PIB model (Cohen et al., 1987) using a Watson sphere charged opposite that of the O ion charge and was spherically averaged with partially occupied 2p states. The radius of the Watson sphere was chosen to give the Madelung potential at the O nucleus in the chosen charge configuration.

Figure 7 shows the difference in integrated charge in each 1.5 Bohr sphere centered around each ion between the PIB charge density and the self-consistent LAPW charge density. There is not a single value of ionicity that agrees perfectly with the self-consistent integrated charges, but an O charge between −1.4 and −1.5 is the best fit. (By separately varying the Watson sphere potential rather than using the Madelung potential, a slightly better

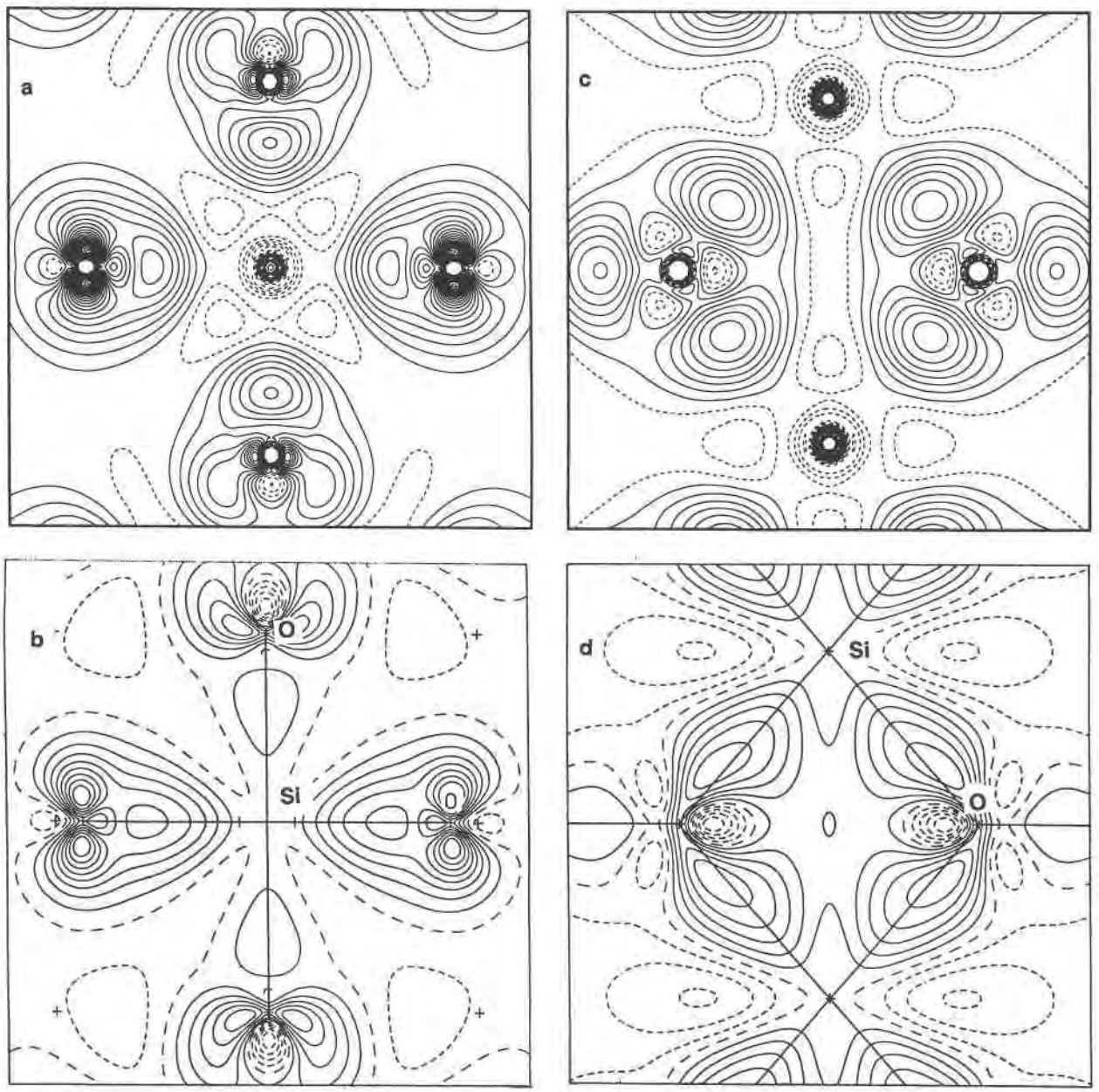

Fig. 6. Deformation densities for stishovite. (**a**) LAPW results for axial-equatorial bond plane (5 Å by 5 Å). (**b**) Experimental model (Spackman et al., 1987, Fig. 7a), same section as **a**. (**c**) LAPW result for shared edge between two SiO_6 octahedra (4 Å by 4 Å). (**d**) Experimental model (Spackman et al., 1987, Fig. 7b), same section as **c**. Contour interval is 0.05 e/Å^3.

fit could be obtained.) Figure 8 shows the differences in the valence band eigenvalues between the potential generated by the PIB charge density and the self-consistent potential at the six k-points that were used for self-consistency. The differences converge at an O charge between -1.2 and -1.4, shifted somewhat to lower ionicity but generally consistent with the ionicity derived from Figure 7. It is impossible to draw more precise conclusions on the ionicity of stishovite by comparing charge densities, but it is clear that the ionicity is reduced from full O^{2-} and Si^{4+} to something like $O^{1.4-}$ and $Si^{2.8+}$. This is very close to the Mulliken charges of -1.2 and $+2.4$ derived from Hartree-Fock calculations (Nada et al., 1990). Note that these static charges should not be confused with the dynamic effective charges appropriate for lattice dynamics (Martin and Kunc, 1981).

Also of interest is how the ionicity changes with pressure. It appears that no major change in ionicity occurs between zero pressure and 143 GPa. At the latter pressure, the best fit obtained for the integrated muffin tin charges is bracketed by O charges of -1.4 and O -1.5, very similar values for zero pressure.

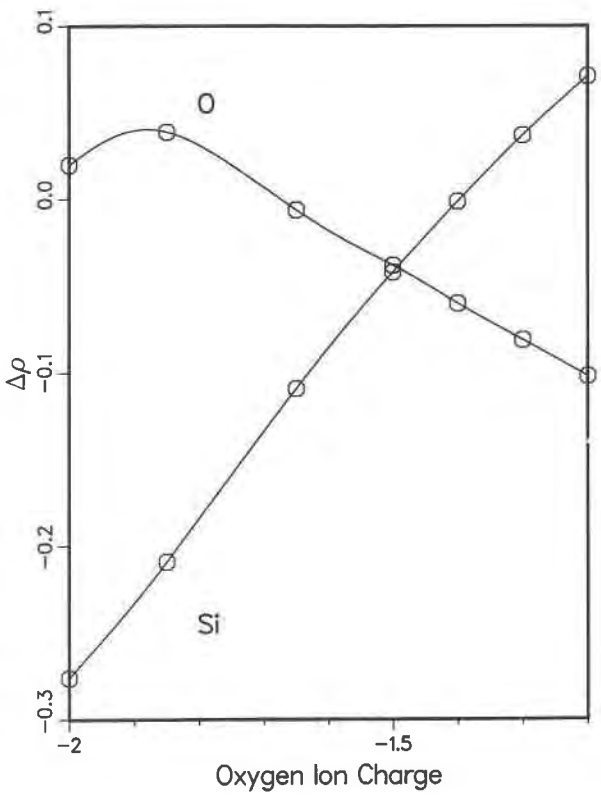

Fig. 7. Difference in muffin tin charges between PIB and LAPW for different assumed O and Si ion charges at zero pressure.

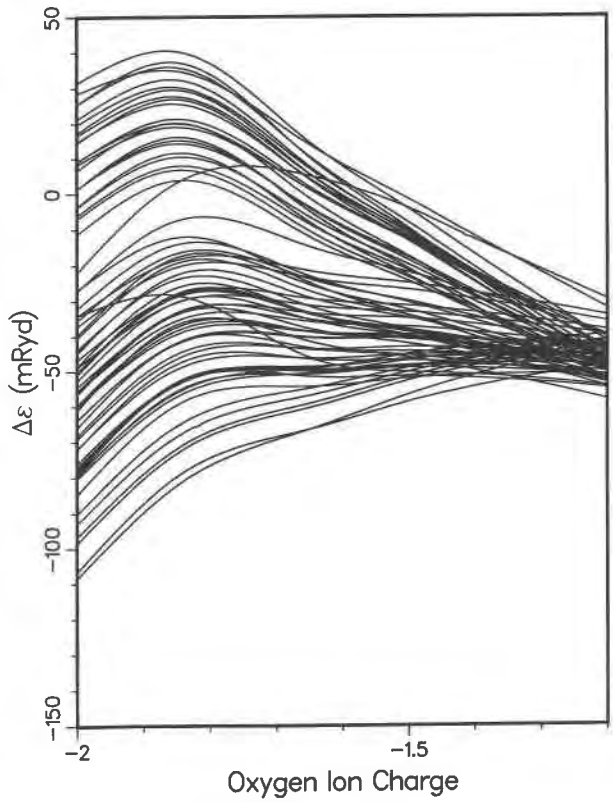

Fig. 8. Differences in valence band eigenvalues of the potential generated by the PIB charge density and the LAPW self-consistent potential at zero pressure.

Difference maps show that the O atoms are very nonspherical. O charge moves out of the shared edge region into the direction perpendicular to the [110] plane of the shared edge and the Si, i.e., out of the bonding regions. This feature is similar to so-called lone pairs but consists of much less than two electrons. To model this feature accurately would require more than a simple shell model, even with multiple shells.

Conclusions

For the first time, elastic constants for a complex crystal with Raman-active modes are calculated using a self-consistent, full potential method, with no uncontrolled approximations other than the LDA. Excellent agreement with experiment is found for the structural properties, the equation-of-state, the linear compressibilities, three elastic constants, and the Raman active A_{1g} mode. Predictions are made for the pressure dependence of some elastic constants. The feasibility of accurately studying elastic and vibrational properties at high pressures from first principles is demonstrated. The discrepancies between the calculated and observed structures at very high pressures (Tsuchida and Yagi, 1989) suggest a reinvestigation of the possible 100-GPa phase transition in stishovite, especially since the interpretation of a phase transition in the diffraction data was based on a small shift in one diffraction line.

Both the charge density and the band structure indicate mixed ionic and covalent character in stishovite, with best fit static charges of $O^{1.4-}$ and $Si^{2.8+}$. The challenge now is to take the results of the total energy calculations and the observations about the charge density to construct a model that can be used to accurately calculate thermal properties and the rest of the elastic constants and vibrational frequencies at high pressures.

Acknowledgments

I owe many thanks to R.J. Hemley for many suggestions and helpful discussions and to M.J. Mehl for discussions regarding elasticity theory. Helpful discussions with W.E. Pickett, D. Singh, H. Krakauer, L.L. Boyer, G.V. Gibbs, G.D. Price, N. Nada, N. Ross, and C.R.A. Catlow are also acknowledged. Special thanks are due to J.B. Thompson, Jr. for suggesting that I "may have to consider the electrons." The computations were performed on the Cray 2 Computer at the National Center for Supercomputing Applications under the auspices of the National Science Foundation.

References cited

Bass, J.D., Liebermann, R.C., Weidner, D.J., and Finch, S.J. (1981) Elastic properties from acoustic and volume compression experiments. Physics of the Earth and Planetary Interiors, 25, 140–158.

Birch, Francis (1952) Elasticity and constitution of the Earth's interior. Journal of Geophysical Research, 57, 227–286.

——— (1978) Finite strain isotherm and velocities for single-crystal and polycrystalline NaCl at high pressures and 300 K. Journal of Geophysical Research, 83, 1257–1268.

Burdett, J.K. (1985) Electronic control of the geometry of rutile and related structures. Inorganic Chemistry 24, 2244–2253.

Chao, E.C.T., Fahey, J.J., Littler, Janet, and Milton, D.J. (1962) Stishovite, SiO_2, a very high pressure new mineral from Meteor Crater, Arizona. Journal of Geophysical Research, 67, 419–421.

Cohen, R.E. (1987a) Calculation of elasticity and high pressure instabilities in corundum and stishovite with the potential induced breathing model. Geophysical Research Letters, 14, 37–40.

——— (1987b) Elasticity and equation of state of $MgSiO_3$ perovskite. Geophysical Research Letters, 14, 1053–1056.

Cohen, R.E., Boyer, L.L., and Mehl, M.J. (1987) Theoretical studies of charge relaxation effects on the statics and dynamics of oxides. Physics and Chemistry of Minerals, 14, 294–302.

Cohen, R.E., Pickett, W.E., and Krakauer, H. (1989a) First-principles phonon calculations for La_2CuO_4. Physical Review Letters, 62, 831–834.

Cohen, R.E., Boyer, L.L., Mehl, M.J., Pickett, W.E., and Krakauer, H. (1989b) Electronic structure calculations for oxide perovskites and superconductors. In A. Navrotsky and D.J. Weidner, Eds., Perovskite: A structure of great interest to geophysics and minerals science, p. 55–66. American Geophysical Union, Washington, DC.

Cohen, R.E., Pickett, W.E., Krakauer, H., and Papaconstantopoulos, D.A. (1990a) High T_c superconductors as ionic metals and the role of phonons in high T_c superconductivity. Phase Transitions, 22, 167–183.

Cohen, R.E., Pickett, W.E., and Krakauer, H. (1990b) Theoretical calculation of strong electron-phonon coupling in $YBa_2Cu_3O_7$. Physical Review Letters, 64, 2575–2578.

Endo, S., Akai, T., Akaham, Y., Wakatsuki, M., Nakamura, T., Tomii, Y., Koto, K., Ito, Y., and Tokonami, M. (1986) High temperature X-ray study of single crystal stishovite synthesized with Li_2WO_4 as flux. Physics and Chemistry of Minerals, 13, 146–151.

Erikson, R.L., and Hostetler, C.J. (1987) Application of empirical ionic models to SiO_2 liquid: Potential model approximations and integration of SiO_2 polymorph data. Geochimica et Cosmochimica Acta, 51, 1209–1218.

Fahey, S., Chang, K.J., Louis, S.G., and Cohen, M.L. (1987) Pressure coefficients of band gaps of diamond. Physical Review B, 35, 5856–5859.

Hedin, L., and Lundqvist, B.I. (1971) Explicit local exchange-correlation potentials. Journal of Physics C, 4, 2064–2083.

Hemley, R.J. (1987) Pressure dependence of Raman spectra of SiO_2 polymorphs: α-quartz, coesite, and stishovite. In M.H. Manghnani and Y. Syono, Eds., High-pressure research in mineral physics, p. 347–359. American Geophysical Union, Washington, DC.

Hemley, R.J., Mao, H.-K., and Chao, E.C.T. (1986) Raman spectrum of natural and synthetic stishovite. Physics and Chemistry of Minerals, 13, 285–290.

Hohenberg, P., and Kohn, W. (1964) Inhomogeneous electron gas. Physical Review, 136 B, 864–871.

Ito, Hisao, Kawada, Kaoru, and Akimoto, Syun-iti (1974) Thermal expansion of stishovite. Physics of the Earth and Planetary Interiors, 8, 277–281.

Kohn, W., and Sham, L.J. (1965) Shelf-consistent equations including exchange and correlation effects, Physical Review, 140 A, 1133–1140.

Lasaga, A.C., and Gibbs, G.V. (1987) Applications of quantum mechanical potential surfaces to mineral physics calculations. Physics and Chemistry of Minerals, 14, 107–117.

Liu, Lin-gun, Bassett, W.A., and Takahasi, Taro (1974) Effect of pressure on the lattice parameters of stishovite. Journal of Geophysical Research, 79, 1160–1164.

Martin, R.M., and Kunc, K. (1981) Direct method of calculation of dynamic effective charges: Application to GaAs. Physical Review B, 24, 2081–2088.

Mehl, M.J., Cohen, R.E., and Krakauer, H. (1988) Linearized augmented plane wave electronic structure calculations for MgO and CaO. Journal of Geophysical Research, 93, 8009–8022; 94, 1977.

Mehl, M.J., Osburn, J.E., Papaconstantopoulos, D.A., and Klein, B.M. (1990) Structural properties of ordered high-melting-temperature intermetallic alloys from first principles total energy calculations. Physical Review B, 41, 10311–10323.

Nada, R., Catlow, C.R.A., Dovesi, R., and Pisani, C. (1990) An ab-initio Hartree-Fock study of α-quartz and stishovite. Physics and Chemistry of Minerals, 17, 353–362.

Nye, J.F. (1985) Physical properties of crystals: Their representation by tensors and matrices, 329 p. Oxford University Press, Oxford.

Olinger, B. (1976) The compression of stishovite. Journal of Geophysical Research, 81, 5241–5248.

Park, K.T., Terakura, K., and Matsui, Y. (1988) Theoretical evidence for a new ultra-high-pressure phase of SiO_2. Nature, 336, 670–672.

Pickett, W.E. (1985) Density functionals in solids, I. Ground state. Communications in Solid State Physics, 12, 1–15.

Ross, N.L., Shu, J.-F., Hazen, R.M., and Gasparik, T. (1990) High-pressure crystal chemistry of stishovite. American Mineralogist, 75, 739–747.

Sato, Yosiko (1977) Pressure-volume relationship of stishovite under hydrostatic compression. Earth and Planetary Science Letters, 34, 307–312.

Schluter, M., and Sham, L.J. (1982) Density functional theory. Physics Today, 35, 36–43.

Schreiber, E., Anderson, O.L., and Soga, N. (1973) Elastic constants and their measurement, 196 p. McGraw-Hill, New York.

Spackman, M.A., Hill, R.J., and Gibbs, G.V. (1987) Exploration of structure and bonding in stishovite with Fourier and pseudoatom refinement methods using single crystal and powder X-ray diffraction data. Physics and Chemistry of Minerals, 14, 139–150.

Stishov, S.M., and Popova, S.V. (1961) New dense polymorphic modification of silica. Geokhimiya, 10, 837–839.

Tsuchida, Yoshihiko, and Yagi, Takehiko (1989) A new, post-stishovite high-pressure polymorph of silica. Nature, 340, 217–220.

Tsuneyuki, S., Tsukada, M., Aoki, H., and Matsui, Y. (1988) First-principles interatomic potential of silica applied to molecular dynamics. Physical Review Letters, 61, 869–872.

Tsuneyuki, S., Matsui, Y., Aoki, H., and Tsukada, M. (1989) New pressure-induced structural transformations in silica obtained by computer simulation. Nature, 339, 209–211.

Wei, S.H., and Krakauer, H. (1985) Local density functional calculation of the pressure induced phase transition and metallization of BaSe and BaTe. Physical Review Letters, 55, 1200–1203.

Weidner, D.J., Bass, J.D., Ringwood, A.E., and Sinclair, William (1982) The single-crystal elastic moduli of stishovite. Journal of Geophysical Research, 87, B4740–B4746.

Wiech, G. (1984) X-ray spectroscopic investigation of the electronic structure of α-quartz and stishovite (SiO_2). Solid State Communications, 52, 807–809.

Manuscript received February 14, 1990
Manuscript accepted March 7, 1991